THE ASTROPHYSICAL JOURNAL, 278:881–892, 1984 March 15

THE ENERGY SPECTRUM OF ELECTRONS AND COSMIC-RAY CONFINEMENT: A NEW MEASUREMENT AND ITS INTERPRETATION[1,2]

K.-K. TANG
Department of Physics and Enrico Fermi Institute, University of Chicago
Received 1983 March 29; accepted 1983 August 25

ABSTRACT

A transition radiation/shower detector telescope with good energy resolution, high detection efficiency, and good background rejection has been used to measure the flux and energy spectrum of cosmic-ray electrons in a balloon flight from Palestine, Texas in 1980. We present our results covering the energy region from 5 to 300 GeV. The spectrum is found to change from $dN/dE \propto E^{-2.7}$ around 10 GeV to $dN/dE \propto E^{-3.5}$ above 40 GeV. We interpret this spectral steepening as the effect of radiative energy losses in interstellar space. A comparison with propagation models indicates that (*a*) electrons are accelerated with an energy spectrum $\propto E^{-2.7}$, (*b*) the confinement time of electrons in the galaxy is about 10^7 yr, and (*c*) the confinement time is independent of energy, and the confinement volume probably includes regions beyond the galactic disk.

Subject headings: cosmic rays: general — particle acceleration — radiation mechanisms

I. INTRODUCTION

High-energy cosmic-ray electrons lose energy as a result of synchrotron radiation in interstellar magnetic fields and of inverse Compton scattering with interstellar photons. The energy loss rate increases with the square of the electron energy and therefore tends to deplete the population of electrons at high energies: one expects to measure a steepening of the electron spectrum when the radiative energy losses dominate over the physical loss through escape from the Galaxy, or when the source regions are so far away that high-energy electrons cannot reach Earth without substantial energy losses. Measurements of the electron spectrum over a large range of energies thus provide information on the containment time of electrons in the Galaxy, on the size of the containment region, and on the spatial distribution of source regions. The interpretation of such measurements does, however, depend on assumptions about the energy spectrum at the acceleration site, which is not known *a priori*.

Successful measurements of the electron spectrum require that (1) the instrument be able to measure the electron energy accurately for a wide range of energies; (2) the experiment be capable of rejecting the copious background of protons, which can interact in the detector to simulate electron events; (3) because of the low flux, the instrument have high detection efficiency as well as a large exposure factor. Meeting all these requirements is a difficult experimental task, which was first attempted in the pioneering work of Anand, Daniel, and Stephens (1971). This and several other experiments to measure the high-energy electron spectrum (Zatsepin 1971; Müller and Meyer 1973; Buffington, Orth, and Smoot 1975; Meegan and Earl 1975; Silverberg 1976; Badhwar, Daniel, and Stephens 1977; Freier, Gilman, and Waddington 1977; Nishimura *et al.* 1981) have, however, led to controversial results.

In 1975, the Laboratory for Astrophysics and Space Research, University of Chicago (Hartmann, Müller, and Prince 1977*a*, *b*), was the first to use a telescope which incorporated a combination of an electronic shower detector and a transition radiation detector. The shower detector, consisting of three scintillators in 8 radiation lengths (51 g cm^{-2}) of lead, measured the electron energy and also rejected a portion of the proton background. The necessary additional background-rejection power was provided by the transition radiation detector. The light weight of the transition radiator made it possible to construct a balloon-borne instrument with large area. The response of this instrument over the energy range from 5 GeV to 300 GeV was calibrated at Fermilab. Figure 1 shows the electron spectrum obtained with this instrument from a balloon flight in 1975 (Prince 1979) compared with the results of other recent investigations. There are still considerable discrepancies among different observations. We therefore have modified our earlier instrument and have performed a new measurement, which will be described in this paper.

In our earlier measurement, the transition radiation detector proved to be essential for the identification of electrons. However, the performance of the instrument could be improved: the energy resolution of the shower detector was relatively coarse, and the data analysis required severe efficiency corrections. We have therefore replaced the original shower detector with a sandwich consisting of nine scintillators in an 18.5 radiation length (118 cm^{-2}) thick stack. We also improved the spatial resolution of the transition radiation detector. These modifications led to very good energy resolution of the instrument, combined with a much improved background-rejection capability and a high acceptance efficiency for electrons. In the following, we shall present our results from a balloon flight of this instrument in 1980, compare our new set of data with the results of previous work, and discuss the astrophysical implications.

[1] This work is supported in part by National Aeronautics and Space Administration grant NSG 7464.
[2] Submitted to the Department of Physics, University of Chicago, Chicago, Illinois, in partial fulfillment of the requirements for the Ph.D. degree.

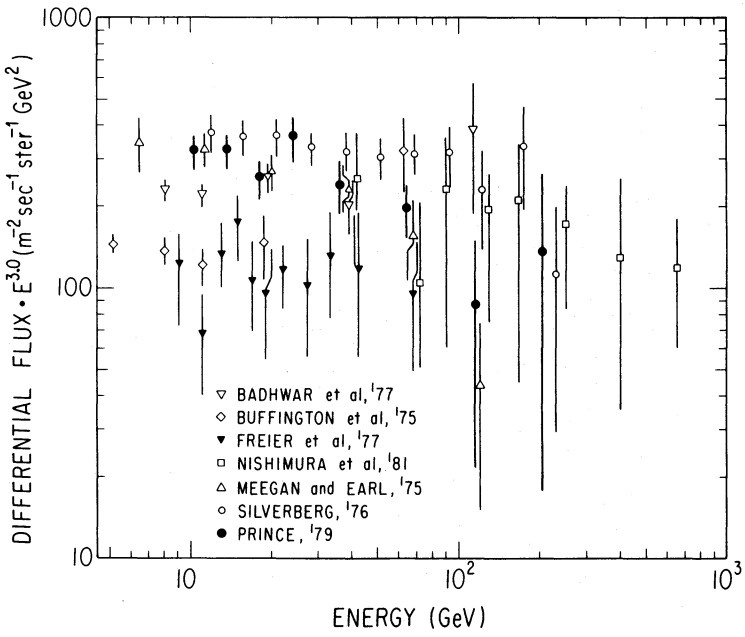

FIG. 1.—Recent measurements of the differential energy spectrum of electrons multiplied by E^3

II. INSTRUMENTATION

A cross section of the instrument used for this experiment is shown in Figure 2. For each particle traversing the telescope, the following parameters are measured: (1) the charge of the particle, (2) its transition radiation signal, (3) its trajectory, (4) the shower profile, and (5) the direction of traversal.

The charge of a particle entering the telescope is measured with plastic scintillator T1 (1 cm thick NE 110, viewed by six RCA 8575 photomultiplier tubes). The signals from the tubes are summed, and the pulse height is analyzed.

The transition radiation signals and the hodoscopic information are obtained from the transition radiation detector, which consists of a sandwich of six radiators and six multiwire proportional chambers (MWPC) and was originally constructed by Hartmann, Müller, and Prince (1977*a*, *b*). The radiators are made of polyethylene foam (Dow Ethafoam), each 14.5 cm thick. Each proportional chamber is 2 cm thick and filled with a mixture of 80% xenon and 20% CO_2. Sense wires, 50 μm in diameter, are spaced 1 cm apart inside the chambers. The signals from groups of adjacent wires are individually amplified and analyzed. For the upper four chambers, each group consists of five adjacent wires forming a strip 5 cm wide. To improve the spatial resolution, the strips in the fifth and the sixth chambers are 4 cm wide (four adjacent wires per strip) and 3 cm wide (three adjacent wires per strip), respectively. A sheet of solid polyethylene (2.5 cm thick) is placed below the lowest proportional chamber to provide some shielding against the backscatter of low-energy shower particles and photons from the lead stack.

The cascade profile is measured with a shower detector whose major components were originally constructed by Müller (1972). The first detector is a CsI plate (D0) of 1 radiation length thickness, viewed by 10 RCA 4516 photomultiplier tubes. D0 is followed by a lead/scintillator sandwich consisting of eight plastic scintillators, D1, ..., D8 (NE 110, 0.6 cm thick each) and seven lead plates (2.5 radiation lengths thick each). The sandwich has a conical shape, its diameter increasing from 49 to 72 cm. Each plastic scintillator is viewed through Lucite light pipes by several RCA 4518 photomultiplier tubes (two tubes each for D1, ..., D4, and three tubes for D5, ..., D8). Signals from photomultiplier tubes belonging to the same scintillator are summed. All photomultiplier tubes have been individually calibrated with a nanosecond light source, and their gains have been adjusted to ensure linearity throughout the entire range of shower sizes. Amplifiers with a semilogarithmic characteristic are used to cover the large dynamic range. The amplified signals for each scintillator are individually processed with pulse-height analyzers of 256 channels each.

The direction of traversal of a particle through the telescope is determined by measuring the time interval between the responses of T1 and D1.

An event is accepted for analysis if it triggers any one of three fast coincidence requirements (E1, E2, and C) formed from the scintillator signals. These coincidences, besides defining the acceptance aperture of the telescope, also serve to reject uninteresting events, thus reducing the dead time for telemetry and pulse-height analysis. For instance, most cosmic-ray protons do not interact in the shower detector and are rejected by high thresholds set for signals from D4 or D6.

The chief coincidence mode, E1, with an acceptance area defined by T1 and D1, requires a positive time of flight (i.e., downward-moving particles) and a D4 signal larger than nine times the average of a singly charged minimum-ionizing particle. This corresponds to the acceptance of electrons above 3.5 GeV with nearly 100% efficiency for all incidence angles within the aperture. The geometric factor is 0.107 m^2 steradian. Mode E2 requires a coincidence between T1 and D5 (with thresholds below the singly ionizing signal), together with a D6 signal above a threshold equivalent to 95 singly charged minimum-ionizing particles. This threshold corresponds to

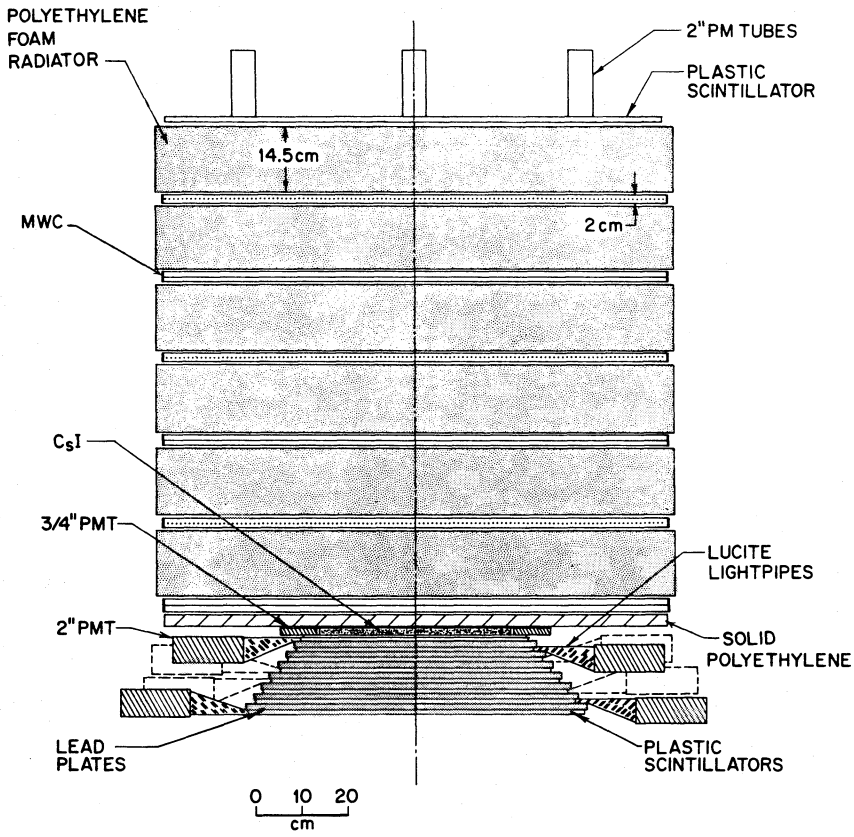

FIG. 2.—Schematic cross section of the instrument

electron energies above 30 GeV. The acceptance aperture, defined by T1 and D5, provides a larger geometric factor (0.148 m^2 steradian) by also accepting events whose trajectories may not traverse some of the counters (D0–D4) above D5.

The calibration mode C requires positive time of flight and signal levels in both T1 and D3 to be larger than 2.3 times the equivalent of a singly charged minimum-ionizing particle. Mode C accepts cosmic-ray nuclei heavier than protons for the purpose of in-flight calibrations.

During the balloon flight, the detector was enclosed in a pressurized gondola. The total weight of the detector with gondola was 1150 kg. All data were transmitted via telemetry to the ground station for on-line analysis and storage on magnetic tape.

III. TECHNIQUES

An essential requirement of this experiment is the ability to efficiently identify electrons from a large background of protons and to precisely measure the energies of the electrons. This is achieved by employing simultaneously a shower detector and a transition radiation detector. In the following, some physical principles and empirical results pertinent to these two techniques will be summarized.

a) Shower Detector

A relativistic electron initiates an electron-photon cascade within a mean depth of 1 radiation length (1 r.l. = 6.37 g cm^{-2} in lead). The profile of the cascade is reconstructed by measuring the ionization with scintillators located at various depths in the lead. The shower detector used in this experiment, with a depth of 18.5 r.l. of lead, has been calibrated with electrons with energies from 2 to 15 GeV at the Standford Linear Accelerator (Fig. 3; Müller 1972). An empirical formula was derived (Müller 1972) to extrapolate the energy dependence of the shower profiles up to 1000 GeV. The validity of this extrapolation was later verified (Prince 1979) at Fermilab with electrons with energies up to 300 GeV.

The measured pulse-height profiles enable one to identify an electron event and deduce its energy by comparing the measured signals with the expected responses using a least-squares fit procedure.

Because of their comparatively long interaction length (175 g cm^{-2} = 27 r.l. in lead), most protons traverse the shower detector without interaction. Still, the main source of background in this experiment is occasional cascades due to interacting protons. Such cascades may be indistinguishable from electron showers, especially if a neutral pion is produced within the first radiation length. The ability of the shower detector to distinguish electron showers from nuclear events depends on how extensively and meticulously it samples the shower profiles. In the earlier experiment (Hartmann, Müller, and Prince 1977*a*, *b*) which used three scintillators and 8 r.l. of lead, about 8% of the cosmic-ray protons produced shower signals indistinguishable from electron showers. With the deeper (18.5 r.l.) shower detector in the present experiment, the fraction of such protons has been reduced to about 2%.

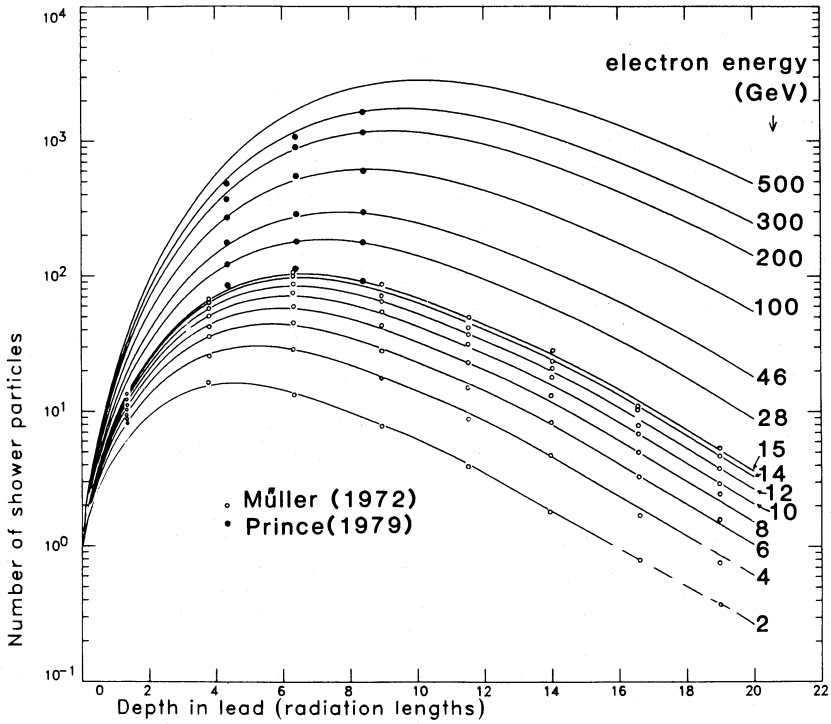

FIG. 3.—Average shower profiles for electrons. The data points between 2 and 15 GeV were measured at SLAC (Müller 1972), and the data points above 15 GeV were measured at Fermilab (Prince 1979). The solid lines represent fits to the measured data with the primary energy as the only free parameter (Müller 1972).

Further, the deeper shower detector has also led to an improvement in energy resolution for electrons (8% standard deviation at ~10 GeV).

b) *Transition Radiation Detectors*

When a relativistic particle passes through alternate layers of media of different dielectric constants, it may generate transition radiation. The yield of this radiation in the form of X-ray photons depends on the Lorentz factor ($\gamma = E/mc^2$) of the particle. The X-ray photons traveling in the forward direction (mean angular spread $\theta \sim 1/\gamma$) can be detected simultaneously with the ionization signal of the particle in a gas proportional chamber. Typically, transition radiation be observed only if the Lorentz factor is very large ($\gamma > 10^3$) (Cherry, Müller, and Prince 1974; Cherry *et al.* 1974). This fact is utilized in our instrument to discriminate between electrons (γ large) and protons (γ small).

The response of our instrument has been calibrated at Fermilab, where the transition radiation detector was placed in particle beams of various Lorentz factors (for details see Prince 1979). For this detector arrangement, transition radiation becomes significant at $\gamma \sim 2000$ and reaches saturation at $\gamma \sim 10^4$. The average signal in saturation is about twice the signal due to ionization alone. In our experiment, all electrons above 5 GeV ($\gamma = 10^4$) produce transition radiation in saturation, while protons below 2000 GeV ($\gamma = 2000$) generate ionization signals only.

Large statistical fluctuations of the transition radiation and ionization signals obtained from a single pair of radiator and proportional chamber make it necessary to employ several radiator/proportional chamber pairs (six in the present experiment) and to analyze the signals using a maximum likelihood method, which we shall describe later.

IV. DATA ANALYSIS

Data were collected for about 20 hr under 4 g cm^{-2} of residual atmosphere in a balloon flight from Palestine, Texas, in 1980. In order that electron events (>3.5 GeV) are recorded without bias with nearby 100% efficiency at the trigger level, the raw data also include events due to interacting nuclei and other background. The subsequent selection of electron events from the recorded data set is based on measurements of the charge, the tracks in the multiwire chambers, the shower profiles, and transition radiation signals. Since this selection is not performed in real time but applied to recorded data with the aid of a computer, we have the flexibility to choose judiciously a wide range of criteria for the above selections. We shall describe the selection criteria and illustrate their effectiveness.

a) *Correction for Instrumental Effects*

First, the trajectories traced by charged particles in the multiwire proportional chambers are reconstructed. With this hodoscopic information, spatial nonuniformities of the detectors are determined by mapping out their responses to cosmic-ray muons at ground level. Corresponding corrections are then applied to the flight data. The track information is also used to determine the angle of incidence of each particle and therefore to determine the amount of detector material (path length) traversed by the particle.

The gain factors for photomultiplier tubes, electronic amplifiers, and gas proportional chambers have been calibrated

on the ground before and after the flight. Singly charged particles as well as cosmic-ray nuclei recorded in-flight are analyzed to check for any temporal gain shifts. No such gain shifts have been observed for the scintillator signals. However, the gains of the proportional chambers were found to increase gradually during the flight at a rate of about 5% per hour, probably due to a slight decrease in gas pressure. Normalizations have been applied to the data to correct for these gain shifts.

b) *Charge Selection*

The signal in the top scintillator, T1, is proportional to the square of the charge of the traversing particle. Accepted electron events must exhibit pulse heights in T1 that are smaller than 2.2 times the most probable pulse height of a relativistic singly charged particle. In this way, multiply charged particles giving rise to larger pulse heights are easily rejected, while electrons are accepted with an efficiency higher than 90%.

c) *Track Selection*

Track information is also used as a selection criterion to reject background events. The MWPC responses yield for each trajectory three measurements of the x-coordinate and three measurements of the y-coordinate. The cleanest events exhibit just a single signal in each multiwire chamber, defining a straight primary trajectory in both projections. Additional signals from wires aside from the primary track, however, do occur as a result of secondary particles. Such secondary particles may be delta-rays or products of nuclear interactions in the material of the detector or in the atmosphere above, or they can be particles or photons scattered backward from the shower detector. For instance, we have found that the events with negative time-of-flight measurements (i.e., upward moving) almost never show a clean trajectory. Their most likely origin is the debris from interacting particles that enter the lead stack from the side.

The identity of an event characterized by a "dirty" trajectory cannot be very well determined. Therefore, accepting only the "clean" events will improve the confidence with which electrons are selected. On the other hand, this decreases the acceptance efficiency and therefore enhances the statistical and systematic uncertainties of the measurement. In view of this, the data analysis has been carried out with three different sets of track selection criteria, denoted by TS1, TS2, and TS3. All three selections require that there must be at least one straight track defined by six wire signals, one in each chamber. In cases when there is more than one straight track, the track with the largest total pulse height is taken to be the trajectory of the primary particle. In addition, TS1 only accepts events with a total of at most four wires fired in each projection. TS2 admits at most two wire signals in each chamber, and TS3 admits at most three wire signals in each chamber. Thus, TS1 selects the cleanest tracks, while TS3 accepts more "dirty" tracks to achieve a higher efficiency.

The data analysis has been performed for each of the three different track selections. The results were found to be consistent with each other. We therefore are confident that the track selection requirements do not introduce significant systematic errors.

d) *Shower Analysis*

In order to identify an electron event in the shower detector and to deduce its energy, the shower profiles measured in the experiment are compared with the expected responses. The measured information for each event consists of the pulse heights s_j ($j = 0, \ldots, 8$) from scintillators D0, D1, ..., D8, and the zenith angle θ.

We define the goodness of fit X^2, as a function of two variables, E, the electron energy, and t_s, the depth at which the shower initiates:

$$X^2(E, t_s) \equiv (N-1)^{-1} \sum^{N} \frac{[n(E, t_s + t_j/\cos\theta) - s_j \cos\theta]^2}{\sigma(E)^2},$$

where $n(E, t)$ denotes the expected number of shower electrons at primary energy E and depth t (in radiation lengths), with expected variance $\sigma(E)$; t_j is the vertical depth of scintillator D_j; and N corresponds to the number of scintillators traversed by the particle in the shower detector. Most results of this experiment are obtained from events which pass through all nine scintillators ($N = 9$). However, in order to obtain better statistics for electrons above 100 GeV, we also analyze the events (coincidence mode E2) whose trajectories miss some of the upper scintillators.

The quantities E and t_s are varied until $X^2(E, t_s)$ reaches a minimum value: $X^2_{\min} \equiv \chi^2$. The value of E that corresponds to χ^2 is taken to be the energy of the primary electron. A selection for electrons can be made by rejecting events with χ^2 exceeding a cutoff value χ^2_{cut}, which must be chosen such that the selection discards most protons but few electrons. We shall discuss the choices of χ^2_{cut} in more detail later.

It is found from accelerator tests that an electron shower most likely starts at $t_s = 0$, and that the probabilities for late showers decrease roughly as $\exp(-t_s)$, t_s in r.l. Therefore, the shower analysis has been performed with the restriction that $t_s < 2.5$ r.l. Alternatively, the analysis has also been performed with a modified goodness-of-fit parameter: $\tilde{X}^2(E, t_s) = X^2(E, t_s) + |t_s|$, which incorporates the probability distribution of t_s so that no further cut on t_s is necessary. We have found no discrepancies between the results from these two approaches.

e) *Transition Radiation Analysis*

A maximum likelihood method has been developed to analyze the signals of the transition radiation detector (Cherry, Müller, and Prince 1974). A singly charged particle generates a set of six signals x_i ($i = 1, \ldots, 6$) along its trajectory in the six proportional chambers. Whether this particle is an electron (producing transition radiation) or a proton (no t.r.) is parameterized by the relative likelihood L, which using Bayes's theorem of probabilities, can be written as

$$L = \prod_{i=1}^{6} P_e^i(x_i)/P_p^i(x_i),$$

where if $p_p^i(x_i)$ is the probability that a proton generates a pulse height x_i in the ith proportional chamber ($i = 1, \ldots, 6$), while $p_e^i(x_i)$ is the probability that an electron generates pulse height x_i.

The probability distributions $P_e^i(x_i)$ and $P_p^i(x_i)$ have been determined by measuring the response of the multiwire proportional chambers to beams of known particles in

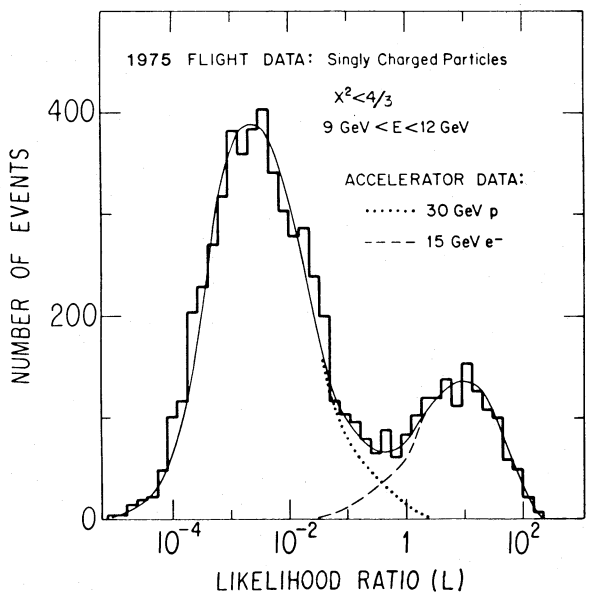

FIG. 4.—Likelihood ratio distribution for 1975 flight data (Prince 1979). The likelihood ratio is a measure of the strength of the transition radiation signal.

accelerator tests (Prince 1979). As will be discussed later, these distributions can also be obtained from the data recorded in flight.

f) *L Distribution and* χ^2 *Cuts*

We expect from accelerator calibrations that the L distributions of protons and electrons show distinct peaks at $L < 1$ and $L > 1$, respectively. Data from a mix of protons and electrons, obtained in a previous balloon experiment (Hartmann, Müller, and Price 1977*a*, *b*), are shown in Figure 4. Obviously, the uncertainty in determining the fraction of electrons in this mixture is due to the overlap of the two distributions. The smaller the fraction of protons in the data set, the smaller the uncertainty is. Since in the energy region of concern, cosmic-ray protons are at least 100 times as abundant as electrons, transition radiation analysis alone is at most marginally sufficient for electron selection, and we have to utilize the results of the analysis of the shower detector (χ^2 selection) in order to further restrain the data set. Such χ^2 selections have been applied to the data shown in Figure 4 from our previous experiment. In Figure 5, we show corresponding histograms obtained in the present experiment. It is evident by comparing Figure 4 with Figure 5 that the present shower detector, with 18.5 r.l. of lead, is more effective in reducing the proton contaminations than the 8 r.l. shower detector of the previous experiment. The unambiguous separation of electrons from protons in the present experiment is also demonstrated in Figure 6, a two-dimensional contour plot with respect to both χ^2 and L.

When we accept events of energy $\gtrsim$90 GeV, which traverse only 10 r.l. of lead and four scintillators (trigger mode E2), we increase the geometric factor at the expense of proton discrimination power. Nevertheless, at these energies, the transition radiation analysis is still quite effective in rejecting

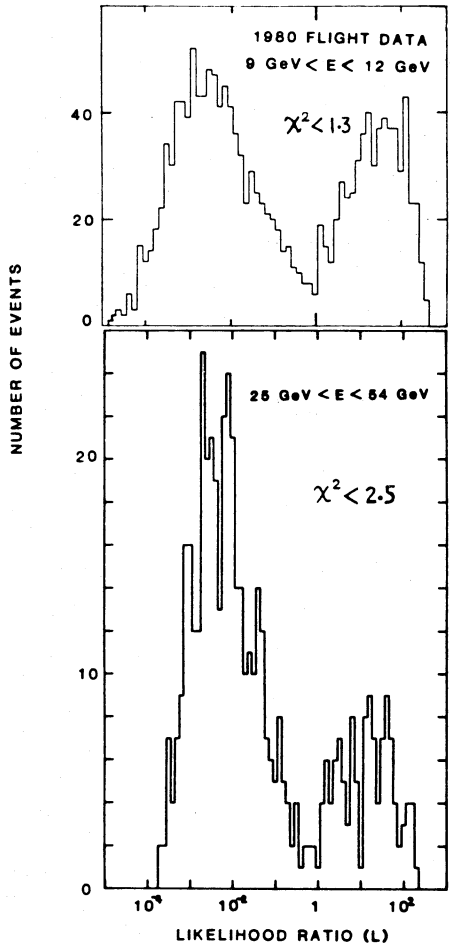

FIG. 5.—Likelihood ratio distributions for flight data of this experiment

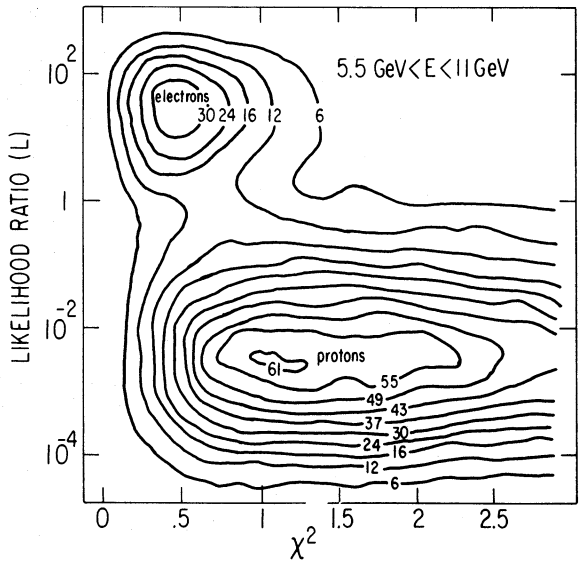

FIG. 6.—Correlation plot of the transition radiation likelihood ratio vs. the χ^2 parameter of the shower fit for a sample of flight data.

TABLE 1

ACCEPTANCE EFFICIENCIES

Energy (GeV)	ΔE (GeV)	$\bar{E}$ (GeV)	f_{T1}	f_{χ^2} ($\chi^2 < 2.5$)	f_{TS1}	f_{TS2}	f_{TS3}	G Exposure Factor (m^2 sr · s)
4.4–5.5	1.09	4.89	0.95 ± 0.03	0.99 ± 0.01	0.48 ± 0.02	0.76 ± 0.03	0.90 ± 0.015	1074
5.5–7.0	1.48	6.16	0.95 ± 0.03	0.99 ± 0.01	0.48 ± 0.02	0.75 ± 0.02	0.90 ± 0.015	1074
7.0–8.9	1.87	7.83	0.95 ± 0.03	0.99 ± 0.01	0.47 ± 0.02	0.75 ± 0.02	0.90 ± 0.015	4723
8.9–11.9	2.94	10.2	0.94 ± 0.03	0.98 ± 0.01	0.45 ± 0.03	0.73 ± 0.02	0.90 ± 0.015	4723
11.9–15.8	3.82	13.6	0.93 ± 0.03	0.97 ± 0.01	0.43 ± 0.03	0.70 ± 0.02	0.90 ± 0.015	4723
15.8–19.0	3.17	17.3	0.92 ± 0.03	0.95 ± 0.01	0.41 ± 0.04	0.68 ± 0.02	0.90 ± 0.015	4723
19.0–25.0	5.89	21.6	0.92 ± 0.03	0.94 ± 0.02	0.38 ± 0.04	0.66 ± 0.02	0.90 ± 0.015	4723
25.0–35.0	9.72	29.2	0.90 ± 0.03	0.92 ± 0.02	0.36 ± 0.05	0.64 ± 0.03	0.90 ± 0.015	4723
35.0–54.0	18.1	42.5	0.89 ± 0.03	0.90 ± 0.03	0.33 ± 0.05	0.61 ± 0.03	0.90 ± 0.015	4723
54.0–100.	41.9	70.1	0.87 ± 0.03	0.84 ± 0.04	0.29 ± 0.05	0.57 ± 0.04	0.90 ± 0.015	4723
88.9–158.	61.4	112.	0.85 ± 0.03	0.75 ± 0.06	0.26 ± 0.05	0.54 ± 0.05	0.90 ± 0.015	7124
158.–281.	109.	200.	0.80 ± 0.03	0.65 ± 0.08	0.19 ± 0.05	0.47 ± 0.06	0.90 ± 0.015	7124

protons, and the errors introduced to the final results remain predominantly statistical.

g) *Computing the Absolute Flux*

We summarize the essential data analysis procedures as follows: (1) selection of singly charged particles; (2) trajectory and time of flight determination; (3) shower analysis to derive χ^2 and energies; (4) grouping the data into different energy intervals; (5) χ^2 selection; and (6) a likelihood analysis for each energy interval. From each L distribution, the number n_e of electron events in the corresponding bin is then deduced.

Finally, we compute the differential energy spectrum of interstellar cosmic-ray electrons. The number of electrons per GeV at energy $\bar{E}$, extrapolated to the top of the atmosphere, is given by

$$\frac{d}{dE} N(\bar{E}) = \frac{n_e f_{\rm atm}}{(G f_{\rm TS} f_{\rm T1} f_{\chi^2} \Delta E)} ,$$

with

$$\bar{E} = \int_{E_1}^{E_2} E^{-\alpha+1} dE \Big/ \int_{E_1}^{E_2} E^{-\alpha} dE ,$$

$$\Delta E = \int_{E_1}^{E_2} E^{-\alpha} dE / \bar{E}^{-\alpha} \qquad (\alpha \approx 3.0) .$$

Here E_1 and E_2 are the lower and upper limits of the energy interval, G is the exposure factor, $f_{\rm atm}$ is the atmospheric correction factor, and $f_{\rm T1}$, $f_{\rm TS}$, and f_{χ^2} are efficiency factors connected with the selections on T1, the track selection, and the χ^2 selection, respectively. We comment on these factors in the following:

The atmospheric correction factor, $f_{\rm atm}$, is caused by bremsstrahlung energy losses of the primary electrons in the residual atmosphere: after passing through h radiation lengths of matter, an electron spectrum of a simple power-law form $dN/dE = aE^{-\Gamma_0}$ will be converted into $dN/dE = (aE^{-\Gamma_0})/f_{\rm atm}$, where $f_{\rm atm} = \Gamma_0^{h/\ln 2}$ (Schmidt 1972). We use $f_{\rm atm} = 1.18$ (for $\Gamma_0 \approx 3.2$ and $h = 0.1$ r.l.) to obtain the electron spectrum at the top of the atmosphere. In order to justify this extrapolation of the measured spectrum, which is not an exact power-law form, we have also used bremsstrahlung formulae (Rossi 1952), to numerically propagate the extrapolated spectrum through 4 g cm^{-2} of air, thus making sure that the constant value of $f_{\rm atm}$ accounts for the atmospheric effect with sufficient accuracy.

Typical values of the selection efficiency factors $f_{\rm T1}$, $f_{\rm TS}$, f_{χ^2}, are shown together with the resulting number of electrons, n_e, in Tables 1 and 2, for three track selections. The error estimates of n_e consist of both the statistical error and the relatively small uncertainties in separating the electrons from the protons in the L distributions. The errors associated with the f-factors include variations such as those due to the particle's angle of incidence. The determination of the f-factors will be discussed in the following section.

IV. DISCUSSION OF THE DATA ANALYSIS

This experiment requires that electrons should be selected unambiguously from the data set, and that the selection should have a high overall efficiency to minimize statistical and systematic errors. These two requirements are mutually incompatible: on the other hand, one can achieve excellent proton-electron separation by imposing strict selection criteria at the expense of reduced efficiency. On the other hand, relaxing the selection criteria for high efficiencies inevitably diminishes the discrimination power against proton background. In the earlier experiment (Hartmann, Müller, and Prince 1977*a*, *b*; Prince 1979), rather stringent track selections were needed to reject background events, and they led to efficiencies well below 50%. The improvements of the instrument for the present experiment made it possible to relax the criteria for both the track selection and the χ^2 selection without significantly impairing the proton discrimination power. Acceptance efficiencies of the order of 90% not only help to reduce the statistical uncertainties, but also help to suppress systematic uncertainties due to errors in the estimation of the efficiency factors.

To evaluate the performance of our instrument, we must study its response to clean and known samples of protons and electrons, respectively. Accelerator beams of electrons, pions, and protons were used to provide such calibrations. However, since the flight conditions differ from the accelerator environment, systematic uncertainties can be minimized if essential detector characteristics can also be derived directly from the flight data. This is feasible because our instrument

TABLE 2

DETECTED NUMBER OF ELECTRONS AND THE ABSOLUTE FLUX

$\bar{E}$ (GeV)	n_e NUMBER OF ELECTRONS FROM EACH TRACK SELECTION			$\bar{E}^3(dN/dE)$ (m^{-2} sr^{-1} s^{-1} GeV^2) FROM EACH TRACK SELECTION			BEST ESTIMATE $\bar{E}^3(dN/dE)$ (m^{-2} sr^{-1} s^{-1} GeV^2)
	TS1	TS2	TS3	TS1	TS2	TS3	
4.89	592 ± 56	935 ± 84	1210 ± 90	155	154	169	155 ± 14
6.16	540 ± 53	860 ± 87	1006 ± 100	207	211	206	208 ± 21
7.83	1931 ± 124	2923 ± 256	3687 ± 220	280	265	279	270 ± 26
10.2	1307 ± 97	2115 ± 104	2556 ± 184	283	282	276	277 ± 17
13.6	690 ± 62	1099 ± 77	1329 ± 101	290	284	267	284 ± 23
17.3	270 ± 33	430 ± 38	589 ± 46	304	292	302	296 ± 29
21.6	243 ± 28	404 ± 30	542 ± 35	315	302	297	302 ± 30
29.2	136 ± 19	242 ± 21	333 ± 25	290	291	284	290 ± 30
42.5	74 ± 14	131 ± 15	180 ± 21	295	282	263	289 ± 36
70.1	22 ± 5	40 ± 8	60 ± 11	213	197	187	220 ± 40
112.	6 ± 3	9 ± 4	16 ± 5	138	100	106	136 ± 40
200.	1 ± 1	2 ± 1.5	2 ± 1.5	122	98	51	102 ± 85

consists of a number of independent detector units. For every event, each of the six transition radiation signals and the shower parameter χ^2 are individually an independent measurement of the liklihood of the event being an electron. Therefore, we can select a specific detector element and study its response to restricted samples of the flight data, provided that the properties of the events in these samples have been unambiguously determined by the remaining detector elements.

We have used this "bootstrap" technique to obtain from flight data the efficiency factors for the track selections and the χ^2 cuts. We have also derived in this fashion the pulse-height distributions used in the transition radiation analysis. Whenever possible, we have checked for self-consistencies and correlations between various measurements, and we have compared the bootstrap results on pulse-height distributions and efficiency factors with those obtained from earlier accelerator tests. No significant disagreements have been found.

For instance, we can select a sample of events with $L \gg 1$ but without any restriction on χ^2. If L is sufficiently large, this sample contains mostly electrons with very little background. Assuming statistical independence between the signals of the transition radiation detector and the shower detector, we then determine efficiency factors f_{χ^2} from the distribution of χ^2 in this sample. The results of f_{χ^2} for $\chi^2 < 2.5$ are shown in Table 1.

The clean separation of electrons from the background depends upon how precisely we have determined, in the likelihood analysis, the pulse-height distributions P_e^i and P_p^i for electrons and protons in the proportional chambers ($i = 1, \ldots, 6$). These distributions can be derived from accelerator test results (Prince 1979). However, some uncertainty remains because the experimental conditions (such as MWPC gain and gas composition) may not be exactly the same in the balloon flight as in the accelerator tests. Therefore, it is advantageous to derive P_e^i and P_p^i from the flight data directly. We also want to derive P_e^i and P_p^i just for events with small χ^2, because we are most interested in the separation of electrons from the interacting protons with electron-like shower signals. To find P_e^i and P_e^j for the jth chamber, we compute for every event a "partial" likelihood ratio:

$$L_j \equiv \prod_{\substack{i=1,\ldots,6 \\ i \neq j}} P_e^i(x_i)/P_p^i(x_i) ,$$

where x_i are the measured pulse heights, and P_e^i and P_p^i ($i \neq j$) are the best estimates of these distributions for the other five chambers. The events with $L \gg 1$ are considered to be entirely electrons, and those with $L \gg 1$ are taken to be entirely non-electron background. The distributions P_e^j and P_p^j can then be obtained from the pulse-height distributions of chamber j for these two types of events, respectively. This procedure is repeated for each chamber j ($j = 1, \ldots, 6$) and is iterated with the improved estimates of P_p^i and P_e^i. We find that these bootstrapped distributions P_p^i and P_e^i lead to better electron-proton separation in the analysis of the flight data than distributions obtained from accelerator tests, although the two sets of distributions differ only slightly.

The track selection efficiencies have been determined as follows. From the flight data, we select a sample of events $S(\chi^2, L)$ on the basis of cuts on the parameters χ^2 and L, and for a specific energy interval. For example, $S(\chi^2 \ll 1, L \gg 1)$ consists almost exclusively of electrons, and $S(\chi^2 \gg 1, L \ll 1)$ consists mostly of background. Thus, for a track selection criterion TS, we obtain an efficiency factor, $f_{\rm TS}(S)$, corresponding to events in S:

$$f_{\rm TS}(S) = \frac{\text{number of events which satisfy TS in } S(\chi^2, L)}{\text{total number of events in } S(\chi^2, L)} .$$

We have derived $f_{\rm TS}(S)$ for track selections TS1, TS2, and TS3, and for S with various selections on χ^2, L, and E. We find that for TS3, the most lenient track selection, $f_{\rm TS3}$ is independent of energy E, but for the more restrictive selections TS1 and TS2, the energy dependence of $f_{\rm TS}$ is significant. We also find that $f_{\rm TS}$ is only very weakly correlated with selections on χ^2 and L. Hence we take $f_{\rm TS}[S(\chi^2 < 1, L > 1)]$ (Table 1) to be the track selection efficiency in the computation of the electron flux. When we determine the

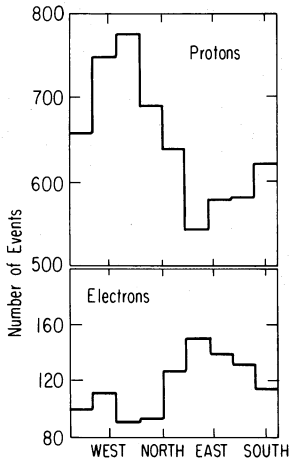

FIG. 7.—Distributions of flight events (with large zenith angles, $E < 10$ GeV) vs. the particles' incoming direction, showing the east-west effect due to geomagnetic cutoffs.

electron spectrum with the three different track selections and their corresponding f_{TS}, we obtain very consistent results (Table 2). This is particularly reassuring since f_{TS1}, f_{TS2}, and f_{TS3} differ substantially in their magnitude as well as in their energy dependence.

For events traversing all nine scintillators in the shower detector, the resolution of electron energy is 8% standard deviation at 10 GeV, and it improves slowly with energy (Müller 1972). Some events triggered with the E2 mode traverse only four scintillators in the shower counter, and the energy resolution is about 15%. Calculations show that the effect of this finite resolution on the absolute flux measurement is less than 3%, which also implies that the shape of the electron spectrum is not affected significantly. We have not applied the correction for this effect to our results.

Below about 5 GeV, geomagnetic cutoff phenomena at the geographic region of this balloon experiment affect the observed spectrum of electrons. The cutoff depends on the sign of the particle's charge, on its rigidity, and on the direction of arrival. We indeed observe the expected east-west asymmetry of fluxes of electrons and protons with energies near 5 GeV (Fig. 7). This result verifies the electron-proton separation and the energy calibration of our detector, even though a quantitative study of the east-west effect is difficult because of the presence of complicated penumbra structures in this geographic region, and because of low statistics of events with large zenith angles. Nevertheless, by restricting the data analysis for the low-energy electrons to particles coming in from easterly directions, we are able to measure the absolute electron flux down to 5 GeV without being affected by the cutoff effects.

VI. RESULTS AND DISCUSSION

The differential energy spectrum of cosmic-ray electrons as obtained in this experiment from 5 to 300 GeV is shown in Figure 8 and in Table 2. The error limits include statistical as well as systematic uncertainties.

For comparison, we have included in Figure 8 the results of Prince (1979), obtained with an earlier version of this instrument, and also the results of a measurement based on different experimental techniques, which was performed by this laboratory (Evenson and Meyer 1981) at lower energies. The excellent agreement among these three measurements strongly supports our confidence in the accuracy of our results.

Figure 8 shows that the shape of the electron spectrum differs significantly from that of cosmic-ray protons, which follows a simple power law ($\propto E^{-2.65}$) at energies above 10 GeV. We are led to believe that this difference is a consequence of radiative energy losses of electrons during propagation. We therefore wish to quantitatively compare our experimental results with the predictions of propagation models. In order to include in our analysis the energy region from 1 to 10 GeV, which is affected by solar modulation, we have extrapolated the interstellar spectrum in this region with the aid of results on the nonthermal radio emission of the Galaxy (Tang and Müller 1982). Such extrapolation helps to impose tighter constraints on the propagation models, although the effect of radiative energy losses is manifest at the high-energy region.

For electrons above 1 GeV, the ionization and bremsstrahlung energy losses in interstellar matter are insignificant. Dominant are energy losses by synchrotron radiation at the rate

$$\frac{dE}{dt_{\rm syn}} = -10^{-16}\langle B^2\rangle \frac{E^2}{8\pi}\ \text{GeV s}^{-1}\ ,$$

where $\langle B^2\rangle$ is the mean square magnetic field in eV cm^{-3}, and by inverse Compton collisions, with (Ginzburg and Syrovatskii 1964; Blumenthal and Gould 1970)

$$\frac{dE}{dt_{\rm Comp}} = -10^{-16}E^2 w_{\rm ph}\left(1 - 6.3\,\frac{E\langle\epsilon^2\rangle}{(m_e c^2)^2\langle\epsilon\rangle} + \cdots\right)\text{GeV s}^{-1}\ ,$$

where $\langle\epsilon\rangle$ and $\langle\epsilon^2\rangle$ are the mean and the mean square photon energy, and $w_{\rm ph}$ is the photon density in eV cm^{-3}. The first term in the Compton loss rate corresponds to the Thomson limit. At electron energies above 5 GeV, the energy loss by scattering with visible and ultraviolet starlight is negligibly small, and the Thomson limit approximation is sufficient for scattering with the 2.7 K radiation and with infrared photons. Therefore, the total energy loss rate for

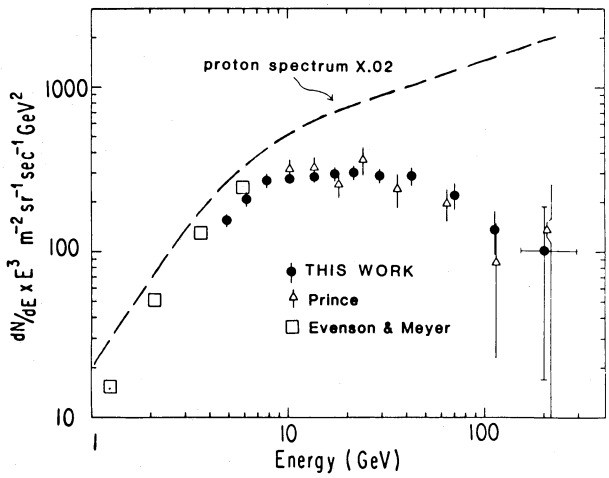

FIG. 8.—The differential energy spectrum of electrons multiplied by E^3. The data points are results from the recent measurements by the University of Chicago. The spectrum of protons is shown for comparison.

TABLE 3

ENERGY LOSS RATE (k) FOR TWO POSSIBLE REGIONS WHERE COSMIC RAYS MAY BE CONTAINED

Confinement Region	w_{ph}(IR) (eV cm^{-3})	w_{ph}(3 K) (eV cm^{-3})	$\langle B^2\rangle/8\pi$ (eV cm^{-3})	k [$= w_{ph}$(IR) + w_{ph}(3 K) + $\langle B^2\rangle/8\pi$] (10^{-16} GeV^{-1} s^{-1})
Disk (half thickness = 300 pc)	0.6–1.	0.25	0.2–0.8	1.05–2.05
Disk + halo (radius = 16 kpc)	0.1–0.3	0.25	0.005–0.05	0.36–0.60

electrons above 5 GeV, including both the synchrotron loss and the Compton loss, is given by

$$\frac{dE}{dt} = -kE^2 \; ; \quad k = 10^{-16}\left(w_{ph} + \frac{\langle B^2\rangle}{8\pi}\right) .$$

Table 3 shows the estimates of the energy loss parameter for two different assumptions of the cosmic-ray confinement region of the Galaxy. The average density of the infrared field is taken from recent estimates by Kniffen and Fichtel (1981). The values for the magnetic fields come from Faraday rotation measurements (Whiteoak 1974) and are consistent with our interpretation of the radio continuum (Tang and Müller 1982).

a) Leaky Box Model

The leaky box, or homogeneous, model assumes homogeneous production and propagation of cosmic-ray electrons throughout the confinement region, and an escape of cosmic rays with an exponential distribution of confinement times (e.g., Ginzburg and Ptuskin 1976). The continuity equation is

$$N(E)/\tau(E) + d/dE[kE^2N(E)] = Q(E) ,$$

where $N(E)$ is the density of electrons of energy E, $\tau(E)$ is the energy-dependent mean containment time, and $Q(E)$ is the source energy spectrum. The forms of the energy dependence of $\tau(E)$ and $Q(E)$ are not known *a priori*. The cosmic-ray proton spectrum suggests a power-law form for $Q(E)$, i.e., $Q(E) \propto E^{-\Gamma_0}$. Cosmic-ray nuclear composition data are consistent with $\tau(E) = \tau_0(E/E_0)^{-\delta}$. With these assumptions, the solution to the continuity equation is (Ramaty 1974)

$$N(E) = E^{-\Gamma_0-1}\int_1^\infty \epsilon^{-\Gamma_0}\exp\left[\frac{-(1-\epsilon^{\delta-1})E^{\delta-1}E_c}{(1-\delta)E_0^\delta}\right]d\epsilon ,$$

where $E_c = (k\tau_0)^{-1}$.

Following the previous work by Prince (1979), we have numerically fitted this solution $N(E)$ to the results of this experiment, treating E_c, Γ_0, and δ as free parameters (Fig. 9 and Table 4). The best fits, which are shown by the shaded area in Figure 9, are characterized by $\delta = 0$, $\Gamma_0 = 2.68 \pm 0.03$, and $E_c = 55 \pm 25$ GeV. We note that the best fit value of Γ_0 turns out to be very close to the power-law index of the cosmic-ray proton spectrum. This may suggest that both species are accelerated with the same spectral shape at the sources. On the other hand, measurements of the secondary to primary ratios of cosmic-ray nuclei have been interpreted (see, e.g., Caldwell 1977; Ormes and Freier 1978) as evidence that $\tau \propto E^{-\delta}$ with $\delta = 0.5 \pm 0.1$. From the electron spectrum we do not find compelling reasons to support such an energy dependence for τ. Curve (c) is the closest fit for $\delta = 0.4$, and it seems to be too flat compared with the measured spectrum.

TABLE 4

NUMERICAL FITS TO THE LEAKY BOX MODEL

Curve	δ	Γ_0	E_c (GeV)	k (10^{-16} GeV^{-1} s^{-1})	$\tau = 1/kE_c$ (10^6 yr)
a.....	0	2.63	32	0.36–0.60 disk and halo 1.05–2.05 disk only	16.5–27.5 4.8–9.4
b	0	2.70	80	0.36–0.60 disk and halo 1.05–2.05 disk only	6.6–11.0 1.9–3.8
c.....	0.4	2.30	7	0.36–0.60 disk and halo 1.05–2.05 disk only	76.–126. 22.–43. (at 1 GeV)

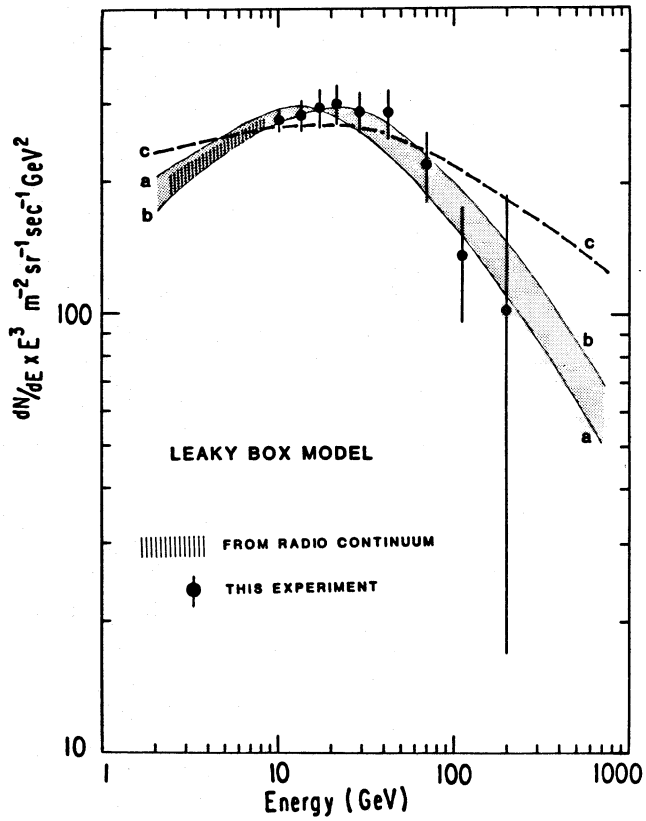

FIG. 9.—The differential energy spectrum of electrons multiplied by E^3. Curved lines are fits to the leaky box model of cosmic-ray propagation. The parameters used to produce the fits are listed in Table 4.

TABLE 5

NUMERICAL FITS TO THE DIFFUSION MODEL

Curve	δ	Halo Radius R_h (kpc)	Source Radius R_s (kpc)	k (10^{-16} GeV^{-1} s^{-1})	Γ_0	Diffusion Coefficient (10^{29} cm^2 s^{-1}) D	$(R_h^2\tau_{Be}/D)^{1/2}$ (10^6 yr) ($\tau_{Be} = 3.8 \times 10^6$ yr)
a	0	16	16	0.36–0.60	2.70	3.3–5.4	29–37
b	0	16	4	0.36–0.60	2.70	12.7–21.2	14–19
c	0.5	16	8	0.36–0.60	2.25	0.7–1.1	50–68 (at 1 GeV)

b) *Diffusion Models*

The propagation of electrons may be described more realistically by the following diffusion equation (see, e.g., Jokipii and Meyer 1968):

$$\frac{d}{dE}[kE^2N(E, \mathbf{r})] - \nabla \cdot [D\nabla N(E, \mathbf{r})] = Q(E, \mathbf{r}) ,$$

where $D = D_0(E/E_0)^\delta$ is the diffusion coefficient, and both the electron density N and the source Q depend on the spatial coordinate $\mathbf{r} = (r, \theta, \phi)$. When one assumes a boundary condition such that $N = 0$ outside a spherical confinement region (the halo) of radius R_h, then the solution N can be represented by summations of spherical Bessel functions j_l and spherical harmonics Y_{l0}. If we also assume that the source function $Q(E, \mathbf{r})$ has a power-law energy dependence and an axially symmetric spatial distribution, i.e., $Q(E, \mathbf{r}) = \tilde{Q}(r, \theta)E^{-\Gamma_0}$, we solve the diffusion equation and obtain the following solution:

$$N(E, r, \theta) = \sum_{l=0}^{\infty} \sum_m Q_{ml} f_m(E) j_l(mr) Y_{l0}(\theta) ,$$

with $m = \lambda_l/R_h$ such that $j_l(\lambda_l R_h) = 0$;

$$Q_{ml} = 2 \int_0^1 d \cos\theta Y_{l0}(\theta) \int_0^{R_h} r^2 dr j_l(mr) \tilde{Q}(r, \theta)/R_h^3 j_{l+1}^2(mR_h) ,$$

$$f_m(E) = E^{-\Gamma_0 - 1} k^{-1} \int_0^1 d\xi \xi^{\Gamma_0 - 2} \exp\left[\frac{E_c(\xi^{1-\delta} - 1)E^{\delta - 1}}{(1 - \delta)}\right] ,$$

$$E_c = D_0 m^2 k^{-1} .$$

Then we fit the numerical solution of $N(E, r = 10$ kpc, $\theta = \pi/2)$ to the observed electron spectrum, treating Γ_0, δ, and D_0/k as free parameters. The quantity $\tilde{Q}(r, \theta)$ is taken to be zero everywhere except at a thin disk, which has a radius R_s and a thickness much smaller than R_s. In our numerical analysis, various values of R_h (radius of the halo) and R_s (radius of the source disk) are tested. A small value of R_s (a few kpc) corresponds to the assumption that all electron sources are located close to the galactic center, while $R_s > 10$ kpc assumes that sources are distributed throughout the Galactic disk, including the solar neighborhood. The best fit results are shown in Figure 10.

Similar to our results in the leaky box approximation, we find that the best fit of our data corresponds to $\delta = 0$ (the shaded area in Fig. 10, Table 5). If we require a diffusion coefficient $D = D_0(E/E_0)^{0.5}$ consistent with the energy dependence of the ratio of secondary to primary nuclei (Ormes and Freier 1978), then all solutions for $N(E)$ appear to be too flat, as shown by curve (c).

By varying the parameter R_s, we can illustrate the effect of the spatial distribution of sources on the shape of the electron spectrum (Fig. 10). For example, curve (b), with $R_s = 4$ kpc, implying the absence of sources near the Sun, would lead to an additional depletion of electrons above 100 GeV. However, although curve (b) seems to fit our data better than curve (a) ($R_s = 16$ kpc), the uncertainty of our measurement above 100 GeV is too large to distinguish the two cases.

c) *Closed Galaxy Models*

If the "source" spectrum of electrons has approximately a simple power-law form, the steepening of the observed spectrum above ~40 GeV unambiguously manifests the competing effects of radiative energy losses and escape from the Galaxy. On the other hand, "closed galaxy" models assume that cosmic rays cannot escape from the Galaxy. Therefore, in these models, the propagation of electrons, in the simplest

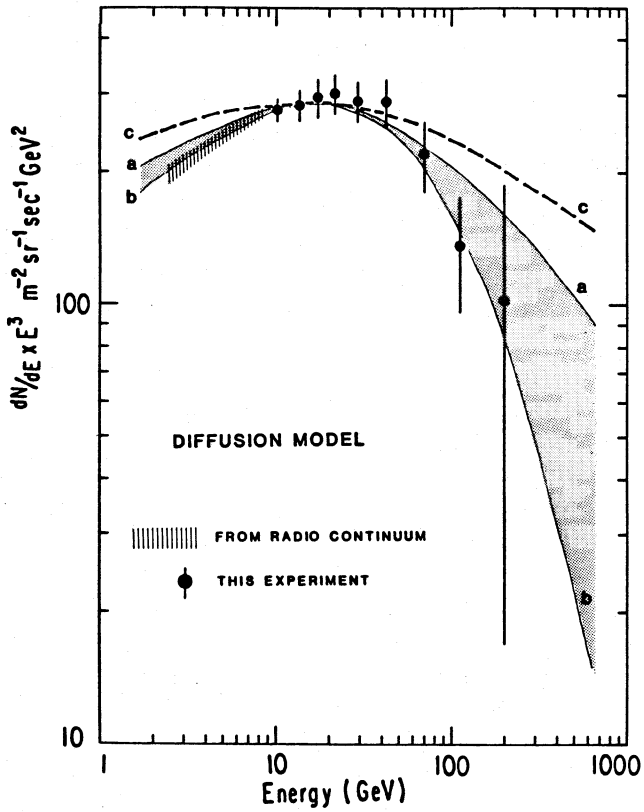

FIG. 10.—The differential energy spectrum of electrons multiplied by E^3. Curved lines are fits to diffusion models of cosmic-ray propagation. The parameters used to produce the fits are listed in Table 5.

case, can be described by setting $\tau(\text{escape}) = \infty$ with the continuity equation: $d/dE[kE^2(N)] = Q(E)$. For a power-law source spectrum: $Q(E) \propto E^{-\Gamma_0}$; the solution to this equation is again a single power law: $N \propto E^{-\Gamma_0 - 1}$, which is, however, inconsistent with our measurement.

d) *Confinement Time and Confinement Region*

On the basis of the measured spectrum of cosmic-ray electrons, we cannot decide whether the leaky box model is sufficient to describe cosmic-ray propagation, or whether more detailed diffusion models must be used. However, in both cases our data are best fit if the propagation mechanism is assumed to be energy independent (i.e., $\delta = 0$). In the leaky box model, we may interpret the steepening of the electron spectrum as a measure of the product of the energy loss rate k and the characteristic confinement time τ. The average value of k depends on the size of the confinement volume (Table 3). The inclusion of a halo in the confinement region implies a smaller energy loss rate. Table 4 gives values for the confinement time τ, corresponding to the numerical fits to our spectrum shown in Figure 9, and for k representative of confinement to the galactic disk or to the disk and halo, respectively. We may compare this result with independent information based on the abundances of the Be isotopes (Garcia-Munoz, Mason, and Simpson 1977; Garcia-Munoz, Simpson, and Wefel 1981), which lead to a confinement time of $13.8(+12.6, -5.0) \times 10^6$ yr. Our results summarized in Table 4 indicate a better agreement with the Be^{10} result if the confinement region includes a halo.[3] A halo is always assumed in the diffusion models. For the comparison with the confinement time obtained from Be^{10}, we use the quantity $(\tau_{Be} R_h^2/D)^{1/2}$, where τ_{Be} is the mean radioactive lifetime of Be^{10} (Prishchep and Ptuskin 1975). As Table 5 and Figure 10 show, fit (b) agrees well with our data and with the Be^{10} results.

Finally, we note that the assumption of energy-dependent confinement, $\tau \propto E^{-\delta}$, $\delta = 0.5 \pm 0.1$, not only leads to a poor fit to the measured spectrum (fit [c] in Fig. 9 and Table 4, and fit [c] in Fig. 10 and Table 5), but also implies a containment time of greater than 4×10^7 yr at 200 MeV, which is inconsistent with the Be^{10} result.

[3] A much stronger argument for the existence of a halo containing cosmic-ray electrons comes from measurements of the diffuse galactic radio emission. The radio intensity from the galactic polar direction is only slightly lower than the intensity from the anticenter direction (see, e.g., the compilation by Webber, Simpson, and Cane 1980). Since the line-of-sight emission length includes only ~ 100 pc of the gaseous disk in the polar direction, but several kiloparsecs in the anticenter direction, this result suggests a sizable halo contribution to the polar radio flux.

VII. CONCLUSION

We have described a measurement of the cosmic-ray electron energy spectrum from 5 GeV to 300 GeV, with an absolute uncertainty in the flux level of $\pm 10\%$ at low energies and $\pm 30\%$ at 100 GeV. Compared with an earlier Chicago measurement (Hartmann, Müller, and Prince 1977*a*, *b*), this result represents a successful effort in reducing the errors through improvements on both instrumentation and data analysis. The measured spectrum, which shows good agreement with the earlier measurement and also with the results of Evenson and Meyer (1981) at lower energies, appears to represent the competing processes of radiative energy loss in the interstellar medium and the leakage out of the Galaxy. In the framework of the leaky box model and diffusion models, our result is most consistent with the picture of cosmic-ray electrons spending on the average, independent of electron energy, 10^7 yr in the Galaxy, where they probably propagate in a halo as well as in the galactic disk.

Because of the limitation by statistics, the flux of electrons above 100 GeV is still very uncertain. More data at the high-energy region will be most valuable in (1) imposing tighter constraints on the spatial distribution of source regions, and (2) setting better limits on the energy dependence of the mean containment time. In principle, our instrument is capable of measuring electrons up to at least 1000 GeV. However, such measurements would require more than a week of exposure time in balloon flights.

I wish to thank my faculty adviser, Professor D. Müller, for his support and advice throughout the course of this project. I sincerely appreciate the help and advice of Dr. T. Prince in the design of this experiment. I also wish to thank Mr. W. Hollis, Mr. D. Bonasera, and Mr. G. Kelderhouse for the electronic work, Mr. W. Johnson for the mechanical design and construction, Mrs. L. Glennie for computer programming, and Mr. R. Kroeger and Mr. J. Camp for assistance during the balloon flight. I appreciate the services and support of the National Scientific Balloon Facility for the balloon flight.

REFERENCES

Anand, K. C., Daniel, R. R., and Stephens, S. A. 1971, *Proc. 12th Internat. Cosmic Ray Conf.* (Hobart), **7**, 2556.
Badhwar, G. B., Daniel, R. R., and Stephens, S. A. 1977, *Ap. Space Sci.*, **49**, 133.
Blumenthal, G. R., and Gould, R. J. 1970, *Rev. Mod. Phys.*, **42**, 237.
Buffington, A., Orth, C. D., and Smoot, G. F. 1975, *Ap. J.*, **199**, 669.
Caldwell, J. H. 1977, *Ap. J.*, **218**, 269.
Cherry, M. L., Hartmann, G., Müller, D., and Prince, T. A. 1974, *Phys. Rev.*, **D10**, 3594.
Cherry, M. L., Müller, D., and Prince, T. A. 1974, *Nucl. Instr. Methods*, **115**, 141.
Evenson, P., and Meyer, P. 1981, private communication.
Freier, P., Gilman, C., and Waddington, C. J. 1977, *Ap. J.*, **213**, 859.
Garcia-Munoz, M., Mason, G. M., and Simpson, J. A. 1977, *Ap. J.*, **217**, 859.
Garcia-Munoz, M., Simpson, J. A., and Wefel, J. P. 1981, *Proc. 17th Internat. Cosmic Ray Conf.* (Paris), **2**, 72.
Ginzburg, V. L., and Ptuskin, V. S. 1976, *Rev. Mod. Phys.*, **48**, 161.
Ginzburg, V. L., and Syrovatskii, S. I. 1964, *The Origin of Cosmic Rays* (London and New York: Pergamon Press).
Hartmann, G., Müller, D., and Prince, T. A. 1977*a*, *Phys. Rev. Letters*, **38**, 1368.
Hartmann, G., Müller, D., and Prince, T. A. 1977*b*, *Proc. 15th Internat. Cosmic Ray Conf.* (Plovidiv), **1**, 366.
Jokipii, J. R., and Meyer, P. 1968, *Phys. Rev. Letters*, Vol. 20, No. 14, p. 752.
Kniffen, D. A., and Fichtel, C. E. 1981, *Ap. J.*, **250**, 389.
Meegan, C. A., and Earl, J. A. 1975, *Ap. J.*, **197**, 219.
Müller, D. 1972, *Phys. Rev.*, **D5**, 2677.
Müller, D., and Meyer, P. 1973, *Ap. J.*, **186**, 841.
Nishimura, J., *et al.* (Japan–US Primary Electron Collaboration). 1981, *Proc. 17th Internat. Cosmic Ray Conf.* (Paris), **2**, 94.
Ormes, J., and Freier, F. 1978, *Ap. J.*, **222**, 471.
Prince, T. A. 1979, *Ap. J.*, **227**, 676.
Prishchep, V. L., and Ptuskin, V. S. 1975, *Astr. Space Sci.*, **32**, 265.
Ramaty, R. 1974, in *High Energy Particles and Quanta in Astrophysics*, ed. C. Fichtel and F. B. McDonald (Cambridge: MIT Press).
Rossi, B. 1952, *High Energy Particles* (Englewood Cliffs, N.J.: Prentice Hall).
Schmidt, P. J. 1972, *J. Geophys. Res.*, **77**, 3295.
Silverberg, R. F. 1976, *J. Geophys. Res.*, **81**, 3944.
Tang, J., and Müller, D. 1982, *Bull. Am. Phys. Soc.*, **27**, 533.
Webber, W. R., Simpson, G. A., and Cane, H. V. 1980, *Ap. J.*, **236**, 448.
Whiteoak, T. B. 1974, in *IAU Symposium 60, Galactic Radio Astronomy*, ed. F. J. Kerr and S. C. Simonson III (Dordrecht: Reidel), p. 137.
Zatsepin, V. I. 1971, *Proc. 12th Internat. Cosmic Ray Conf.* (Hobart), **1**, 116.

KWOK-KWONG TANG: Laboratory for Astrophysics and Space Research, The Enrico Fermi Institute, The University of Chicago, 933 East 56th Street, Chicago, IL 60637